Subcellular Distribution of M2-muscarinic Receptors in Relation to Dopaminergic Neurons of the Rat Ventral Tegmental Area

Miguel Garzón[1,2] and **Virginia M. Pickel**[1]

[1]Department of Neurology and Neuroscience, Weill Medical College of Cornell University, New York, NY 10021, USA

[2]Departamento de Anatomía, Histología y Neurociencia, Facultad de Medicina UAM, Madrid, 28029, Spain

Abstract

Acetylcholine can affect cognitive functions and reward, in part, through activation of muscarinic receptors in the ventral tegmental area (VTA) to evoke changes in mesocorticolimbic dopaminergic transmission. Of the known muscarinic receptor subtypes present in the VTA, the M2 receptor (M2R) is most implicated in autoregulation, and also may play a heteroreceptor role in regulation of the output of the dopaminergic neurons. We sought to determine the functionally relevant sites for M2R activation in relation to VTA dopaminergic neurons by examining the electron microscopic immunolabeling of M2R and the dopamine transporter (DAT) in the VTA of rat brain. The M2R was localized to endomembranes in DAT-containing somatodendritic profiles, but showed a more prominent, size-dependent plasmalemmal location in non-dopaminergic dendrites. M2R also was located on the plasma membrane of morphologically heterogenous axon terminals contacting unlabeled as well as M2R or DAT-labeled dendrites. Some of these terminals formed asymmetric synapses resembling those of cholinergic terminals in the VTA. The majority, however, formed symmetric, inhibitory-type synapses, or were apposed without recognized junctions. Our results provide the first ultrastructural evidence that the M2R is expressed, but largely not available for local activation, on the plasma membrane of VTA dopaminergic neurons. Instead, the M2R in this region has a distribution suggesting more indirect regulation of mesocorticolimbic transmission through autoregulation of acetylcholine release and changes in the physiological activity or release of other, largely inhibitory transmitters. These findings could have implications for understanding the muscarinic control of cognitive and goal-directed behaviors within the VTA.

Keywords

Acetylcholine; reward; cognition; synapse; electron microscopy

Introduction

Muscarinic cholinergic receptors in the ventral tegmental area (VTA) are prominently involved in both cognition and reward (Yeomans, 1995; Yeomans and Baptista, 1997; Ikemoto and Wise, 2002; Ikemoto et al., 2003; Miller et al., 2005). The cognitive actions are largely attributed to muscarinic modulation of VTA dopaminergic neurons projecting to the

*Correspondence to: Dr. Miguel Garzón, Department of Anatomy, Histology and Neuroscience, Medical School UAM, Arzobispo Morcillo 4, 28029 Madrid, Tel: (34) 91-497-5466, Fax: (34) 91-497-5353, Email: miguel.garzon@uam.es.

prefrontal cortex. In contrast, VTA dopaminergic neurons projecting to the nucleus accumbens and other limbic targets are most highly implicated in reward and emotional responses also affected by activation of muscarinic receptors in the VTA (Forster and Blaha, 2000; Greba et al., 2000). Changes in the sensitivity of dopamine D1/D2 receptors during cocaine withdrawal may be mainly due to M2R activation (Ushijima et al., 2000). Together, these observations indicate the crucial importance of understanding the cellular sites for modulation of dopaminergic transmission through activation of muscarinic receptors in the VTA.

Cholinergic input to the VTA originates in the mesopontine cholinergic nuclei (Henderson and Sheriff, 1991; Oakman et al., 1995) and potently excites VTA dopaminergic neurons (Lacey et al., 1990; Gronier and Rasmussen, 1998). Moreover, muscarinic activation of VTA neurons increases dopamine release in their cortical and limbic target territories (Niijima and Yoshida, 1988; Westerink et al., 1996, 1998; Enrico et al., 1998). Both these actions are consistent with our demonstration that cholinergic terminals form mainly asymmetric, excitatory-type synapses on VTA neurons, some of which express varying levels of the dopamine transporter (DAT) (Garzón et al., 1999). The VTA cholinergic terminals, however, more frequently, contacted non-dopaminergic neurons (Garzón et al., 1999) that are largely GABAergic (Steffensen et al., 1998). The cholinergic activation of VTA GABAergic neurons could result in collateral inhibition of dopaminergic neurons and increased GABA release in cortical and limbic brain regions receiving GABAergic projections from the VTA (Van Bockstaele and Pickel, 1995; Carr and Sesack, 2000). These observations suggest a highly complex and cell-type specific cholinergic modulation of neurons in the VTA that may be mediated through several receptor subtypes.

Five muscarinic receptor genes have been cloned (Kubo et al., 1986; Bonner et al., 1987, 1988; Peralta et al., 1987), and their receptors have been localized in the rat brain (Levey et al., 1991). Pharmacological and behavioral studies in mice lacking functional M2 receptors (M2R) have shown the involvement of the M2R in central muscarinic actions such as antinociception, hypothermia and tremor (Gomeza et al., 1999, 2001; Wess et al., 2003). M2R involvement in cognition (Comings et al., 2003) is supported by M2R-selective antagonists effects, such as spatial memory enhancement or cognitive improvement in Alzheimer disease (Clader & Wang, 2005; Youdim & Buccafusco, 2005). The M2R has a subcellular distribution consistent with actions as a presynaptic auto- and hetero-receptor and a postsynaptic receptor in several different brain regions (Rouse et al., 1997, 1998, 2000). Mesocorticolimbic dopaminergic flow is known to depend partially on muscarinic activation (Forster and Blaha, 2000, 2003). Together, these observations suggest that dopaminergic neurons within the VTA are subject to regulation by cholinergic agents that bind the M2R. The cellular mechanisms mediating the actions of M2R ligands in the VTA are, however, unclear. Furthermore, there is no ultrastructural evidence for the specificities of targeting of M2R to dopaminergic neurons or their afferents in this region. Thus, to address these questions we examined the electron microscopic immunocytochemical localization of antipeptide antisera against M2R and dopamine transporter (DAT) in single sections through the rat VTA.

Material and Methods

Antisera

The M2R immunoreactivity was detected with a rabbit polyclonal antiserum (product number AMR-002, Lot AN-08, Alomone Labs Ltd, Jerusalem, Israel). This antiserum was directed against a synthetic fusion protein containing Glutathione S-transferase fused to a part of the i3 intracellular loop of human M2R (residues 225-356) (Bonner et al., 1987; Peralta et al., 1987; Levey et al., 1991). The identity of the fusion protein was confirmed by

DNA sequence and SDS-PAGE Western blotting of rat brain membranes. In order to verify the value of this antiserum for immunohistochemistry, its specificity for the immunogen peptide (product number AMR-002, Lot AN-08, Alomone Labs Ltd, Jerusalem, Israel) was tested in the rat VTA. The M2R antiserum (1μg/ml) was added to an excess of the immunogen fusion protein (3μg/mg) and incubated with gentle agitation for 24 hr at 4°C. Sections were then processed by using solutions of M2R antiserum, pre-adsorbed M2R antiserum, or incubation buffer without antiserum. As additional controls for selective recognition of the M2 receptor, sections through the VTA of two M2R knockout (Gomeza et al., 1999) and two adult wild-type mice were examined for immunoperoxidase labeling using the M2R antiserum. Since knockout mice are known to sometimes show developmental compensations for loss of a required protein, we also included sections through the VTA from two M5R knockout mice (Yamada et al., 2001) to serve as additional positive controls. The null mice were adult (3 weeks) males (129/J1, CF1-M2r stock #789 and 129/S6, CF1-M5R stock #1261) supplied by Taconic farms (Germantown, NY). The observed presence of M2R immunolabeling in both wild-type and M5, but not M2 knockout mice is consistent with specificity of the antiserum for the M2R.

A commercially available rat monoclonal antibody raised against DAT (Catalog number MAB369, Chemicon, Temecula, CA) was used for the immunocytochemical labeling of dopaminergic neurons in the VTA. This antibody is directed against the N-terminus (residues 1-66) of the human DAT (Pristupa et al., 1994) fused to Glutathione S-transferase (GST) (Ciliax et al., 1995); its specificity has been exhaustively demonstrated by immunoblot analysis studies with cloned and native brain proteins (Ciliax et al., 1999; Hersch et al., 1997, Miller et al., 1997). The DAT antibody has been characterized by Western blot analysis, in which it recognized its fusion protein, without cross-reactivity to GST (Hersch et al., 1997). Additional characterization and specificity tests were done by immunoblotting using a stable SK-N-MC cell line expressing human DAT, untransfected SK-N-MC cells, and HeLa cells transiently expressing either the human serotonin or norepinephrine transporters; in these experiments, the DAT antibody recognized a single protein band of 85-KD molecular weight in the stable SK-N-MC cell line expressing DAT (Hersch et al., 1997; Miller et al., 1997), with no cross-reactivity to the serotonin and norepinephrine transporters (Miller et al., 1997). Thus, in rat brain membranes, the antibody binds to a single protein band with the same mobility as the cloned transporter (Hersch et al., 1997)

The specificity of the DAT antibody was also characterized by immunohistochemistry in brain tissue (Hersch et al., 1997; Ciliax et al., 1999). The distribution of the DAT antibody in rat brain agreed with known dopamine cell groups and their projections, and was identical to the distribution observed using polyclonal antibodies (Ciliax et al., 1995). Moreover, specificity of this antibody for DAT has been also tested by immunostaining brain sections from rat and monkey that received unilateral nigrostriatal lesions with 6-hydroxy-dopamine and 1-methyl-4-phenyl-1,2,3,6-tetrahydropyridine [MPTP], respectively (Hersch et al., 1997; Ciliax et al., 1999). Those neurotoxic lesions completely abolished DAT immunoreactivity in striatal regions ipsilateral to the lesion (Hersch et al., 1997; Ciliax et al., 1999).

In addition, we also tested specificity for secondary antisera in our particular experimental conditions in control experiments by replacing the M2R and the DAT antisera with normal sera, which produced no detectable labeling.

Tissue preparation

Preparation of the tissue prior to immunocytochemistry was done according to procedures described by Leranth and Pickel (1989). All efforts were made to minimize animal suffering,

and to use the minimal necessary number of animals. The experimental protocol strictly conformed with National Institutes of Health guidelines for the Care and Use of Laboratory Animals and was approved by the Institutional Animal Care and Use Committee of Joan and Sanford I. Weill Medical College and Graduate School of Medical Sciences of Cornell University. Four (250-300 g) male Sprague-Dawley rats (Taconic, Germantown, NY) were deeply anesthetized with 100 mg/kg i.p. sodium pentobarbital. The brains were fixed by aortic arch perfusion with (1) 20 ml of heparin (1000 U/ml) in saline, (2) 50 ml of 3.8% acrolein (Polysciences, Warrington, PA) in a solution of 2% paraformaldehyde in 0.1 M phosphate buffer (PB; pH=7.4), and (3) 200 ml of 2% paraformaldehyde in 0.1 M PB. The six mice used for immunolabeling specificity control experiments (two wild-type, two M2R knockout and two M5R knockout) were anesthetized and perfused using a similar protocol to that of the rats. The exceptions in mice include perfusion through the left ventricle of the heart, and reduction of the volume of acrolein to 20 ml and the 2% paraformaldehyde to 100 ml. Both rat and mouse brains were removed from the cranium, dissected and postfixed for 30 minutes in 2% paraformaldehyde. Coronal sections were collected through the midbrain region including the VTA. These were cut at 40-50 μm thickness into 0.1 M PB at 4°C on a Leica Vibratome VT1000 S (Leica Instruments GmbH, Nussloch, Germany). These sections of tissue were incubated for 30 minutes in a solution of 1% sodium borohydride in 0.1 M PB to remove excess of active aldehydes, and rinsed in 0.1 M PB until bubbles disappeared. To enhance the penetration of immunoreagents, the sections were then cryoprotected for 15 minutes in a solution of 25% sucrose and 3% glycerol in 0.05 M PB, frozen quickly in liquid chlorodifluoromethane (Freon, Refron Inc., NY) followed by liquid nitrogen, and thawed in 0.1 M PB at room temperature. After extensive rinsing in 0.1 M Tris-buffered saline (TS; 0.9% NaCl in 0.1 M Tris, pH=7.6), the sections were incubated for 30 minutes in 0.5% bovine serum albumin (BSA) in 0.1 M TS to minimize nonspecific staining, and then processed for dual-immunocytochemical labeling.

Immunocytochemistry

Rat brain sections prepared as described above were processed for dual immunocytochemical detection of M2R and DAT using a protocol described by Chan et al. (1990). The primary antisera against M2R and DAT were raised in rabbits and rats, respectively, and therefore could be recognized by appropriate species-specific secondary antibodies. Most of the sections were processed for immunogold detection of M2R and immunoperoxidase detection of DAT, since the immunogold method gives a more precise subcellular localization of the receptors than the immunoperoxidase method. In two animals, peroxidase and gold labels were switched in some sections, however, in order to verify the distribution of the receptor using two markers known to differ in resolution and sensitivity (Leranth and Pickel, 1989). Sections prepared as described above were incubated for 36-42 hours at 4°C in a solution containing: (1) rabbit polyclonal antiserum for M2R (diluted 1:100 for immunogold or 1:2,000 for immunoperoxidase) and (2) rat monoclonal antibody for DAT (diluted 1:2,000 for immunogold and 1:20,000 for immunoperoxidase). After incubation in these primary antisera, sections were first processed for immunoperoxidase and afterwards for immunogold labeling. All the incubations were carried out at room temperature with continuous agitation on a rotator and were followed by several rinses in 0.1 M TS, 0.1 M PB and 0.01 M phosphate-buffered saline (PBS; 0.9% NaCl in 0.01 M PB, pH=7.4).

For the immunoperoxidase visualization of antigens, the avidin-biotin complex (ABC) method (Hsu et al., 1981) was used for dual labeling in rat or for single labeling in either rat or mouse tissue. For this, the incubation in primary antisera was followed by incubation in secondary biotinilated antibody (goat anti-rat IgG for DAT, Chemicon, Temecula, CA, or goat anti-rabbit IgG for M2R, Vector Laboratories, Burlingame, CA; 1:400) for 30 minutes

and then in ABC (1:100, Vectastain Elite Kit, Vector Lab.) for another 30 minutes. The immunoreactivity bound to the tissue was visualized by a 6 minute incubation in 0.022% 3,3′-diaminobenzidine and 0.003% hydrogen peroxide in 0.1 M TS, pH=7.6.

The sections used for dual labeling were then prepared for silver-enhanced immunogold labeling by the method of Chan et al. (1990). Thus, they were rinsed in 0.1 M TS, transferred to 0.01 M PBS, blocked for 10 minutes in 0.8% BSA and 0.1% gelatin in 0.01 M PBS, and incubated for 2 hours in colloidal gold (1 nm)-labeled antibody (goat anti-rat IgG for DAT, Electron Microscopy Sciences, Fort Washington, PA, or goat anti-rabbit IgG for M2R, Amersham, Arlington Heights, IL, 1:50). After this, the sections were fixed for 10 minutes in 2% glutaraldehyde in 0.01 M PBS and reacted with a silver solution IntenSE™M kit (Amersham, Arlington Heights, IL) for either (1) 4-7 minutes for electron microscopy, or (2) 10-12 minutes for light microscopy. Sections processed from rat or mouse brain for light microscopy were rinsed in 0.05 M PB and mounted on glass slides. After overnight drying in a dessicator, they were dehydrated through immersion in a series of increasing-concentration alcohols, and defatted in xylene (J.T. Baker, Phillipsburg, NJ). Finally, the slides were coverslipped and examined using a Nikon Microphot-FX light microscope (Nikon, Garden City, NY) equipped with a digital CoolSNAP camera (Photometrics, Huntington Beach, CA). The acquired images were equally adjusted for contrast and brightness using Photoshop 6.0 software.

Electron microscopy

Immunolabeled sections for electron microscopy were postfixed in 2% osmium tetroxide in 0.1 M PB for one hour, dehydrated through a series of graded ethanols and propylene oxide, and incubated overnight in a 1:1 mixture of propylene oxide and Epon (EMbed-812; Electron Microscopy Sciences, Fort Washington, PA). The sections were transferred to 100% Epon for 2 hours and flat-embedded in Epon between two sheets of Aclar plastic (Allied Signal, Pottsville, PA). Ultrathin sections (40-50 nm) were cut from the outer surface of the tissue with a diamond knife (Diatome, Fort Washington, PA) by using an ultramicrotome (Ultratome, NOVA; LKB-Productor AB, Bromma, Sweden). The regions examined were located in the VTA at the levels of anteroposterior planes -5.2 to -5.6 mm from Bregma of the rat brain atlas of Paxinos and Watson (1986). The sections were collected on 400-mesh copper grids, counterstained with uranyl acetate and lead citrate (Reynolds, 1963), and examined with a Tecnai Biotwin 12 (Serial # D271) electron microscope (FEI Company, Hilsboro, OR).

Only sections near the surface of the tissue at the Epon-tissue interface were examined in order to reduce false negatives due to inadequate penetration of antisera. The classification of identified cellular elements was based on the descriptions of Peters et al. (1991). Axon terminals were identified by the presence of numerous synaptic vesicles and were at least 0.2 μm in diameter. Small unmyelinated axons were <0.2 μm and rarely contained small vesicles. Neuronal somata were identified by the presence of a nucleus, Golgi apparatus, and rough endoplasmic reticulum. Dendrites usually contained abundant endoplasmic reticulum, and were distinguished from unmyelinated axons by their larger diameter and/or abundance of uniformly distributed microtubules. In addition, dendrites were in many cases postsynaptic to axon terminals. The term "somatodendritic profiles" was used to design the pooled number of neuronal somata and dendrites, expressing the whole population where M2R activation might occur at postsynaptic sites within VTA neurons. Asymmetric synapses were recognized by thick postsynaptic densities (asymmetric synapses, type Gray I), while symmetric synapses had thin pre- and post-synaptic specializations (symmetric synapses, type Gray II) (Gray, 1959). Zones of closely spaced parallel plasma membranes, which lacked discernible synaptic densities, but were otherwise not separated by glial processes, were defined as appositions or nonsynaptic contacts, and were not included in the

quantification unless specifically stated. A profile was considered to be selectively immunoperoxidase labeled when it contained cytoplasmic precipitates making it appear more electron dense than morphologically similar profiles located within the same section. A profile was considered to contain immunogold labeling when two or more gold particles were observed within large profiles. However, in dendrites less than 0.5 μm diameter and in small unmyelinated axons a single particle was considered positive immunogold-labeling, since almost no gold-silver deposits were seen over myelin and other tissue elements not known to express muscarinic receptors. The validity of this approach was established previously (Garzón et al., 1999). In dendrites, the particles were considered extrasynaptic when located > 50nm away from the edge of the nearest postsynaptic specialization (Fig. 2) and perisynaptic when detected on plasmalemmal surfaces ≤ 50nm away from these synaptic borders, regardless of the dendritic size.

The ultrastructural quantitative analysis was carried out in 15 vibratome sections with M2R-immunogold and DAT-immunoperoxidase labeling that were obtained from four animals. All immunoreactive processes (n=3084) were counted in randomly sampled electron micrographs at magnifications of 4,500-30,000 × from an area of 9,776.8 μm^2, with an area of at least 1,420.3 μm^2 examined in each animal. The tissue was quantitatively examined to determine the relative frequencies with which the immunoreactive products were localized within neuronal somata, dendrites, axons or glial cells. In addition, morphologically recognizable synaptic relationships of each labeled profile were also quantified, as well as non-synaptic appositional contacts among M2-immunoreactive and/or DAT-labeled profiles. ANOVAs were used to determine whether there was significant variability in total labeled profiles per square micron of analyzed surface with respect to different animals. Variations in the density (mean number per cross-sectional surface unit) of asymmetric and symmetric synapses established by either M2R-immunolabeled terminals or M2R-immunoreactive dendrites were assessed using Student t-tests. To evaluate the localization of M2R labeling in plasmalemmal versus cytoplasmic sites in VTA dendrites, M2R immunogold particles density (number of particles/analyzed surface) within these compartments were calculated; data were collected independently for dendrites showing cross-diameter >1μm or <1μm in both single-M2R and dual-DAT+M2R dendrites. Batteries of Chi-square tests were applied to the data obtained from dendrites immunoreactive for M2R to assess the statistical association among pairs regarding (1) M2R subcellular distribution, (2) dendritic size and (3) presence of concomitant DAT-immunolabeling in those profiles.

The electron micrographs used for the figures were acquired with an AMT digital camera (Advanced Microscopy Techniques Corporation, Danvers, MA) on a Microsmart Computer using a Windows 2000 operating system. Adobe Photoshop (version 7.0; Adobe Systems Inc., Mountain View, CA), Canvas (version 8.0.4; Deneba Systems, ACD Systems, Miami, FL) and Adobe Illustrator (version 9.0; Adobe Systems, Inc.) software programs were utilized for adjustment of contrast and brightness, and to build and label the composite illustrations.

Pre-embedding immunocytochemistry achieves good ultrastructural preservation of the tissue and assures the identification of antigens that are sensitive to plastic embedding, but has limited penetration of immunoreagents (Leranth and Pickel, 1989). Thus, differential penetration of gold versus peroxidase in dual-labeling procedures may contribute to an underestimation of the number of labeled profiles and/or frequency of associations. Therefore, to achieve valuable quantitative analysis of dual-labeling in sections processed before plastic embedding, and to minimize the probability of false negatives, we (1) freeze-thawed the tissue sections to enhance penetration of immunoreagents, and (2) only collected ultrathin sections near the resin-tissue interface, having most complete access to immunoreagents. We also used the immunoperoxidase and immunogold-silver markers for

M2R receptor detection in order to obtain more optimal information on both subcellular distribution and frequency of associations. These precautions greatly enhanced the method reliability and partially overcame its limitations. Thus, although the quantitative values may underestimate the total number of profiles containing M2R and DAT, they provide a good relative comparison of the cellular and subcellular distribution of the labeling patterns.

Results

DAT immunoreactivity was seen by light microscopy in many somata and extending dendrites in the rat VTA. No such labeling was seen in absence of the primary anti-DAT antibody. In contrast, M2R immunoreactivity in rat VTA was distributed homogeneously throughout the neuropil, and was often associated with varicose processes presumed to be axons (Fig. 1A). Either omission of the M2R primary antiserum (data not shown), or adsorption of this antiserum with the corresponding immunogenic fusion protein resulted in the complete disappearance of the specific staining pattern in rat VTA (Fig .1B). Immunoreactivities for M2R within the VTA of both wild-type (Fig. 1C) and M5R knockout mice (Fig. 1E) were similar to normal rats, and not seen in mice without expression of M2R (Fig. 1D). The M2R immunoreactivity appeared slightly more intense in the M5R knockout, compared with wild-type mice, which may reflect compensation for loss of the M5 receptor, or methodological variations in perfusion fixation.

Electron microscopy confirmed the localization of M2R immunoreactivity in somatodendritic as well as axonal profiles within the VTA. Differences were observed in the intensity of labeling for M2R when using peroxidase and gold markers. As compared with immunogold, the high sensitivity of the immunoperoxidase method allowed detection of M2R immunoreactivity in more small profiles and particularly small unmyelinated axons and glial processes, but the peroxidase localization of M2R to precise organelles was less certain than that seen using immunogold. The global distribution of M2R labeling in different cellular compartments with either method was, however, rather similar, and there were no apparent differences in frequencies or types of associations between differentially labeled profiles. Therefore, for the statistical analysis, we used only numbers obtained from the tissue in which M2R was detected with the immunogold method allowing precise subcellular resolution and DAT was detected with the immunoperoxidase method. Illustrations are, however, shown also with M2R-immunoperoxidase labeling.

ANOVA showed that there was statistically significant differences in the total number of M2R-immunoreactive profiles per analyzed unit area among different animals ($F_{3,501}$=13.351; p<0.001), most probably reflecting differences in perfusion fixation. Separate ANOVAS for each cellular compartment, however, indicated an absence of significant differences among animals in any of them except M2R-labeled glial processes ($F_{3,501}$=2.778; p<0.05). The pattern of labeling and the cellular associations between M2R-labeled profiles were also similar in all cases. Thus, although there were significant inter-animal variations in the density of immunoreactivity among animals, the data was pooled from different animals in the following descriptive analysis. A summary table of the M2R and/or DAT immunolabeled neuronal profiles is provided (Table 1).

Somatodendritic M2R distribution

In somatodendritic profiles, M2R immunoreactivity was distributed heterogeneously within the cytoplasm, and frequently localized to endomembranes resembling smooth endoplasmic reticulum (Fig. 2). In these somata, the M2R-immunogold particles were associated with Golgi lamellae (Fig. 2), or more rarely located on portions of plasma membrane adjacent to incoming afferents, as was also often seen in dendritic profiles (Figs. 3,4). M2R labeling within neuronal cell bodies represented only 2.5% (n=31 of 1236) of the M2R-

immunoreactive profiles. In contrast, 58% (n=746 of 1236) of all M2R-labeled profiles were dendrites most often ranging from 1.0 - 2.5 μm in diameter.

The M2R-immunogold labeling was mainly located on plasma membranes within dendrites ≤1μm (Fig. 3A), but a more cytoplasmic distribution resembling that of somata was observed in larger dendrites (Fig. 2B). Most of the dendritic plasmalemmal particles were seen on portions of the plasmalemma not receiving synaptic input from axon terminals. Only 1.4% of the observation of M2R-immunogold was seen within synaptic specializations (1.4%) (Fig. 4). The predominant plasmalemmal distribution of M2R-immunogold labeling in M2R-immunolabeled dendrites was quantitatively confirmed; thus, ANOVA showed significantly higher M2R-immunogold density (mean number of gold particles per dendrite) associated to the plasma membrane (1.47±0.11) in comparison to the cytoplasm (0.95±0.12) in M2R-labeled dendrites ($F_{1,14}=10,85$; p<0.0054). The prominent localization of M2R-immunolabeling to the plasma membrane was related to the dendritic size (ANOVA for interaction dendritic size × immunogold subcellular distribution: $F_{1,12}=35.07$; p<0.001), being exclusive of VTA dendrites <1μm; in dendrites >1μm plasmalemmal and cytoplasmic localization of M2R-immunogold labeling did not differ significantly. Analysis of the M2R immunogold in randomly sampled dendrites showed that almost 80% of the total dendritic gold particles were in contact with the plasma membrane in small dendrites (<1μm). Statistical significant association among dendritic size and location of M2R-immunolabeling was also confirmed using the Chi-square test for the raw number of M2R-immunogold particles in those randomly sampled M2R-labeled dendrites ($X^2_1=69.3$; p<0.001).

The M2R-immunoreactive dendrites received both symmetric (n=253; 62%) and asymmetric (n=155; 38%) synapses. Terminals containing M2R comprised approximately 8% (n=31) of the total inputs to M2R-immunolabeled dendrites. The remaining inputs were almost exclusively from unlabeled axon terminals (over 90%) (Figs. 2,3,4), although a few afferent axon terminals contained detectable DAT immunoreactivity (Fig. 4A). The statistical analysis showed that symmetric synaptic density was significantly higher than asymmetric synaptic density when referring to synapses made between either unlabeled terminals ($t_{504}=3.691$; p<0.0002) or total axon terminals (unlabeled plus M2R- and/or DAT-immunolabeled) ($t_{504}=4.166$; p<0.0001) and M2R-immunoreactive dendrites.

M2R and DAT distributions in separate, apposed or single dendrites

The dendritic profiles immunolabeled for M2R were dispersed within a neuropil containing many DAT-labeled somata and dendrites (n=1935 total DAT-immunolabeled profiles) (Table 1). Most of these labeled dendrites were separated from each other by glial processes, small axons, and axon terminals differentially terminating on either the DAT or M2R-labeled dendrites (Fig. 3A). In some cases, however, differentially labeled dendrites had apposed plasmalemmal surfaces, and were contacted by a single common afferent terminal (Fig. 3B). Nineteen percent of single M2R-labeled dendrites (n=132;19.5%) were apposed to DAT-immunoreactive dendrites. In M2R-immunoreactive dendrites, the labeling was usually located on portions of the plasma membrane distant from DAT-labeled apposing dendrites, and often near glial profiles or incoming synaptic inputs from axon terminals (Fig. 5).

Approximately 10% of the M2R-immunogold labeled dendrites (n=78 out of 746) or somata (n=3 out of 31) contained DAT-immunoperoxidase reaction product (Table 1). The M2R subcellular distribution in dually-labeled dendrites was qualitatively distinct from that seen in M2R single-labeled dendrites. In contrast to the mainly plasmalemmal M2R labeling in exclusively M2R-labeled dendrites (Figs. 3,4), M2R-immunogold in the DAT-labeled dendrites had a mostly cytoplasmic distribution (Fig. 6). Two-way ANOVAs (factors: subcellular distribution × labeling type) showed statistically significant variations in the

mean M2R-immunogold density (distribution: $F_{1,28}=9.69$; $p<0.0045$; distribution $\times$ labeling: $F_{1,28}=74.09$; $p<0.0001$) (Fig. 7). Post-hoc comparisons with the Fisher's test revealed that in the dually labeled profiles M2R-immunogold density was higher in the cytoplasm compared to the plasma membrane both in large (Fig. 6A,B) and small (Fig. 6C,D) dendrites. In contrast, plasmalemmal M2R-immunogold density was significantly higher in the plasma membrane in the M2R single-labeled dendrites (Figs. 5,7). Chi-square test for the number of M2R-immunogold particles in those randomly sampled dendrites showed a statistically significant association among M2R subcellular distribution (cytoplasmic vs. plasmalemmal) and the type of labeling (dual vs. single) ($X^2_1=158.9$; $p<0.0001$), and this occurred regardless of the dendritic size (Table 2). A statistically significant association was also observed between dendritic size and M2R subcellular distribution in single M2-labeled dendrites, but not in dually DAT+M2R-labeled dendrites, since cytoplasmic labeling was consistently higher regardless of dendritic size in the dually-labeled dendrites (Fig. 7, Table 2). Finally, Chi-square test for M2R-immunogold particles showed an absence of statistically significant association between the type of labeling (dual vs. single) and the dendritic size (diameter <1μm vs diameter >1μm) ($X^2_1=1.85$; $p<0.25$) (Table 2). Furthermore, the slight plasmalemmal M2R labeling in DAT-immunolabeled dendrites was hardly ever located near incoming axon terminals, but on portions of the plasma membrane far away from afferent inputs, unlike the distribution of M2R-immunogold particles in dendrites without DAT immunoreactivity. Dendrites containing both M2R and DAT received symmetric and asymmetric inputs mainly from unlabeled terminals (Fig. 6).

M2R distribution in axonal profiles

Small unmyelinated axons (n=166) and axon terminals (n=231) containing M2R-immunogold comprised 32% (n=397) of the total M2R-labeled processes in the VTA (Fig. 8, Table 1). M2R-immunolabeled unmyelinated axons were ≤0.2 μm in diameter and rarely contained small synaptic vesicles. In contrast with the diffuse axonal distribution of M2R-immunoperoxidase labeling (Fig. 8C), M2R-immunogold particles were prominently localized to the plasma membrane in the small axons (Figs. 4A,6C) as well as in axon terminals (Fig. 8). A few M2R-labeled myelinated axons were also detected. About 60% of the M2R-immunogold particles within axon terminals were localized at sites on or near the cytoplasmic surface of the plasma membrane.

The M2R-labeled terminals differed in their size (0.3-1.4 μm diameter) and types of associations with other neuronal or glial profiles (Figs. 8,9). These associations included axodendritic synapses (Fig. 8) as well as appositional contacts with axon terminals and/or glial processes (Figs. 8,9). Most M2R immunogold-labeled terminals contained only densely packed small clear synaptic vesicles (40-60 nm in diameter), and sometimes one or more mitochondria. Occasionally, the labeled terminals contained many small clear as well as a few dense-core vesicles (Fig. 8). Gold-silver particles identifying M2R within axon terminals sometimes contacted synaptic vesicles, but no attempt was made to quantify the frequencies of these associations since the size of the gold particles was usually larger than the vesicles.

Most M2R-immunogold labeled terminals were devoid of DAT immunoreactivity (97.8%; n=226; Table 1); we observed, however, five axon terminals that contained both DAT and M2R immunoreactivities (Fig. 8D). These dually M2R+DAT-labeled axon terminals comprised a small proportion of both M2R-labeled (2.2%, 5/231) and DAT-labeled (8.3%; 5/60) terminals (Table 1).

M2R-distribution in terminals contacting M2R- or DAT-labeled dendrites

M2R-labeled terminals were often without discernible synaptic specializations in the examined plane of section, but some of the terminals did form synaptic junctions with either unlabeled (n=34), M2R-labeled (n= 31), or DAT-labeled (n=9) dendrites. Synapses onto M2R-immunoreactive dendrites were mainly of the symmetric morphology (n=25; 81%) (Fig. 8A) in comparison to asymmetric synapses (n= 6; 19%). A statistically significant higher density of symmetric versus asymmetric synapses was evidenced (t_{504}=2.544; p<0.011) within synapses established between M2R-labeled terminals and M2R-labeled dendrites. The preferential symmetric targeting of M2R-labeled dendrites by M2R-immunoreactive terminals also can be seen from analysis of the labeling in the targets of these terminals. M2R-immunoreactive axon terminals were observed in 10% of the overall symmetric-type synapses onto M2R-labeled dendrites (25 out of 253), but only in 3.8% of the whole asymmetric-type synapses established onto the M2R-labeled dendrites (6 out of 155). The M2R-immunoreactive axon terminals contained immunogold-silver particles that were usually distant from the contacts with the M2R-labeled dendrites (Fig. 8A). In contrast to the prevalence of symmetric synapses on M2R-labeled dendrites, synapses between M2R-labeled axon terminals and unlabeled dendrites showed no statistically significant differences in their symmetric (56%; n=19) or asymmetric (44%; n=15) membrane specializations (t_{504}=0.458; p<0.647).

DAT-immunoreactive somatodendritic profiles (n=1539) were prevalent in the VTA neuropil (Table 1). The DAT-immunolabeled dendrites showed a clear tendency to be preferentially targeted by M2R-immunoreactive terminals. These terminals accounted for almost 5% (56 out of 1164) of the total contacts onto the DAT-containing dendrites, but only 1% of the total contacts onto non-DAT dendrites. The majority of the contacts between M2R-labeled terminals and DAT-labeled or unlabeled dendrites were characterized by apposed plasma membranes without clearly defined synaptic membrane specializations within a single plane of section (Fig. 9). About 24% (n=56) of the M2R-immunoreactive terminals established such appositions on DAT-labeled dendrites. In contrast, only 16% (n=9) of these contacts showed clearly defined synaptic junctions observed (Fig. 8C).

The DAT-immunolabeled dendrites recipient to M2R-immunoreactive terminals also received convergent input from unlabeled terminals and were apposed to many small axonal and glial processes (Fig. 9). The vast majority of the apposing glial processes were unlabeled, although some of them also showed M2R immunoreactivity. Labeled glial processes comprised only about 2% of the total number of M2R-labeled profiles within the VTA.

Discussion

Our results provide ultrastructural evidence that M2 receptors in the VTA have strategic distributions supporting an active involvement in modulation of the postsynaptic excitability of mainly non-dopaminergic neurons. In addition, they confirm and extend earlier studies suggesting a major presynaptic role for M2R in afferent terminals to both dopaminergic and non-dopaminergic neurons including those that also express the M2R in the VTA (Fig. 10). These distributions, together with the observed intracellular location of M2R in a small population of VTA dopaminergic neurons suggests multiple sites where activation of M2 receptors within the VTA circuitry may affect cognitive and rewarding behaviors influenced by mesocorticolimbic projections.

Methodological considerations

The characterization of the DAT antiserum used in this study has been previously reported (Hersch et al., 1997, Miller et al., 1997; Ciliax et al., 1999); it has shown a high specificity for DAT protein and recognizes its antigen in multiple rat brain regions (Ciliax et al., 1999; Svingos et al., 1999, 2001). The M2R-immunogold labeling was located on the cytoplasmic surfaces of plasma membranes, in agreement with the recognition of the i3 intracellular loop of the human cloned M2R gene including the peptidic sequence against which the antiserum was raised (Bonner et al., 1987). Finally, specificity of M2R labeling in the present study is also supported by: (1) absence of labeling in negative control experiments with omission of the M2R antiserum, (2) background control experiments with substitution of the secondary antiserum, (3) immunolabeling absence when the M2R antiserum was preadsorbed with the antigenic peptide against which the antiserum was raised (4) absence of labeling in M2R knockout mice.

M2R subcellular distribution in somata and dendrites: relationship to DAT

We observed M2R immunoreactivity in somatodendritic profiles suggesting local synthesis of this receptor in neurons of the rat VTA. In contrast, however, most studies using *in situ* hybridization reported virtual absence of M2R mRNA in this region (Buckley et al., 1988; Weiner and Brann, 1989; Weiner et al., 1990; Vilaró et al., 1992, 1994); only Levey et al. (1991) reported M2R mRNA in ventral midbrain at levels similar to those in the hippocampal formation or amygdala. This discrepancy may reflect the greater sensitivity of high resolution electron microscopic immunocytochemistry in comparison with *in situ* hybridization or a mismatch between rat and human in the sequence of oligonucleotide probes employed (Buckley et al., 1988).

In somata and proximal dendrites, the M2R labeling was mainly associated with endomembranes that may be involved in the synthesis, transport and/or internalization of the receptors from functional sites on plasma membrane (Broadwell and Cataldo, 1983; Weclewicz et al., 1998; Stowell and Craig, 1999). M2R internalization after binding to specific ligands in early endosomes is known to be a down-regulation mechanism of the receptor availability (Krudewig et al., 2000; van Koppen, 2001). Similar mechanisms of ligand-triggered receptor mobilization have been reported for other G-protein binding receptors (Cahill et al. 2001). The paucity of detectable labeling for M2R on the plasma membranes of VTA perikarya, however, suggests that plasmalemmal binding of M2 Ragonists is unlikely to occur on somata. Cytoplasmic MR2 distribution in non-dopaminergic, as well as some dopaminergic neurons in VTA suggests that MR2 in this region may be synthesized for transport to terminal fields in cortical and limbic territories, where M2 Ractivation modulates presynaptic transmitter release (Vannucchi and Pepeu, 1995; Douglas et al., 2001; Zhang et al., 2002).

In comparison with the proximal dendrites, distal dendrites of mainly non-dopaminergic neurons more frequently showed M2R immunoreactivity in association with extrasynaptic and perisynaptic plasma membranes. This higher proportion of plasmalemmal versus cytoplasmic distribution of M2R in distal dendrites may be due to differences in receptor turnover, trafficking, or internalization rates (Bradbury and Bridges, 1994; Parton et al., 1992). This distribution is comparable to that of M2R in most other brain regions (Hersch et al., 1994; Mrzljak et al., 1998; Erisir et al., 2001). The non-synaptic plasmalemmal M2R distribution may reflect, in part a restricted access of the immunoreagents to the active zone (Nusser et al., 1995). These sites may, however, be those that are functionally active, since M2R, like most other G-protein-coupled receptors have a perisynaptic/ extrasynaptic location when examined with a combination of labeling methods (Baude et al., 1993; Luján et al., 1996). Indeed, extrasynaptic muscarinic receptors show high-affinity for their ligands

and are known to be involved in nonsynaptic transmission in the central nervous system (for review see Vizi, 1998; Vizi and Kiss, 1998). Diffusion of neurotransmitters as far as 1μm from their release sites is able to activate high-affinity nonsynaptic receptors through volume transmission (Asztely et al., 1997). Thus, the observed appositional contacts of M2R-immunolabeled dendrites without bona fide synaptic junctions may be indicative of cellular interactions of functional relevance in the understanding of central cholinergic neurotransmission.

A few of the M2R-labeled somatodendritic profiles in the VTA were either lightly or intensely DAT immunoreactive. Prior studies have suggested that the VTA neurons expressing low levels of DAT are principally those that project to the prefrontal cortex, while those with more intense labeling project to limbic forebrain regions (Garzón et al., 1999). The present localization of M2R in DAT-labeled neurons of the VTA was unexpected, since *in situ* hybridization studies indicate that only M5 mRNA is present in midbrain dopaminergic neurons (Weiner et al., 1990). The M2R labeling in DAT immunoreactive neurons was fairly sparse on plasma membranes, however, and largely associated with cytoplasmic membranes. This distribution suggests that under basal conditions the M2R somatodendritic labeling in the VTA represents non-functional receptors that may show activity-dependent recruitment to functional sites on the dendritic surfaces, as has been shown for M2R receptors in other brain regions (Bernard et al., 1998; Decossas et al., 2003). The M2R transfer to the plasma membrane could enhance receptor activation without new protein synthesis. The somatodendritic M2R in DAT-containing somata and dendrites of the VTA also may undergo trafficking to distant terminals in target regions, since presynaptic M2R receptors have been reported in the cerebral cortex and striatum (Mrzljak et al., 1993; Hersch et al., 1994; Alcantara et al., 2001). In comparison with DAT-immunoreactive neurons, M2R labeling was more commonly seen in somata and dendrites without detectable DAT. These neurons are likely GABAergic, since GABA is present in most non-dopaminergic neurons of the VTA (see introduction). GABAergic neurons in the VTA comprise local circuit neurons and projection neurons of the mesocorticolimbic pathway (Van Bockstaele and Pickel, 1995; Carr and Sesack, 2000).

Subcellular distribution of M2R in axonal profiles of varying morphology

The present localization of M2R to axonal plasma membrane is consistent with physiological experiments suggesting modulation of transmitter release through a G protein-mediated decrease of calcium channel permeability (Dolphin, 1995,1998). The detection of M2R immunoreactivity on vesicular membranes suggests that activation of the receptor also may inhibit calcium-dependent neurotransmitter release directly, most probably through changes in coupling processes between receptor activation and neurotransmitter secretion. Activation of M2 receptors in vesicles might also inhibit neurotransmitter release through mediation of vesicular docking (Bourne, 1988; Mizoguchi et al., 1990). Alternatively, vesicular M2R may reflect transportation to and from functional sites by vesicles, and/or receptor recycling (Broadwell and Cataldo, 1983; Smythe and Warren, 1991; Mukherjee et al., 1997; Sudhof, 2004).

Most M2R-labeled terminals showed appositional contacts with dendrites, but lacked clearly defined synaptic specializations. This suggests that activation of M2 receptors may primarily affect transmitter release from non-synaptic varicose axon terminals (*boutons en passant*), like those described for both cholinergic and monoaminergic neurons in several brain regions (Vizi and Kiss, 1998; Raiteri et al., 1990; Starke et al., 1989). It is also likely, however, that many of the synaptic junctions formed by M2R-labeled terminals were undetected due to the preferential location of M2-immunogold toward the perimeter of axon terminals distant from their dendritic contacts.

Of the detected synapses formed by M2R-labeled terminals, the majority were symmetric. The symmetric synapses are typical of axon terminals containing GABA and/or co-stored opioid peptides in the VTA (Pickel et al., 1993; Sesack and Pickel, 1995). M2 receptors have been implicated in the modulation of GABA release in the cerebral cortex (Ferraro et al., 1997) and the substantia nigra, where the GABAergic terminals mainly originate from striatal projections (Kayadjianian et al., 1994). Our results are the first to suggest the specific involvement of the M2R subtype in the release of inhibitory transmitters in the VTA. These M2R-labeled GABAergic terminals in the VTA may derive locally from interneurons showing somatodendritic labeling for M2R in the present study or from extrinsic regions such as the ventral striatum or ventral pallidum (for review see Grillner and Mercuri, 2002). Muscarinic modulation of GABA release from either of these sources could play an important role in both drug reward and antimuscarinic psychosis (Yeomans, 1995).

In addition to the symmetric junctions, the M2R-labeled terminals also sometimes formed synapses with thickened postsynaptic membrane specializations that are typical of those containing glutamate (Charara et al., 1996; Smith et al., 1996; Paquet et al., 1997; Garzón et al. 1999). Moreover, M2 receptors have been implicate in the modulation of glutamate release in other brain regions (Fukudama et al., 2004; Li et al., 2002). Glutamatergic inputs to the VTA may originate from projection neurons of the cerebral cortex as well as the glutamatergic and/or cholinergic neurons in the mesopontine tegmental region that express M2R mRNA (Phillipson, 1979; Vilaró et al., 1992). Our prior localization of the vesicular acetylcholine transporter in VTA terminals forming asymmetric synapses (Garzon et al., 1999) strongly suggests that at least some of the M2R-labeled terminals forming this type of junction are cholinergic. This conclusion is supported by the well known role of M2R as a muscarinic autoreceptor (Levey et al. 1991; Vilaró et al., 1992, 1994; Kitaichi et al., 1999; Zhang et al., 2002) affecting acetylcholine release in several other brain regions (Kilbinger, 1984; Starke, 1989). Dual labeling of M2R and selective markers for acetylcholine is necessary, however, for the unequivocal identity of the transmitter phenotype of the excitatory-type terminals expressing M2 receptors in the VTA.

The few dopaminergic terminals showing M2R-immunolabeling in the VTA could correspond to axon collaterals of local midbrain neurons projecting to the striatum. Dopaminergic neurons in the substantia nigra compacta and retrorubral field emit axons showing varicosities and terminal boutons when traversing VTA in its route to dorsal striatum (Prensa and Parent, 2001). DAT-immunolabeled terminals have been reported previously in the VTA, although they are much less prevalent than dopaminergic dendrites, (Garzón et al., 1999).

Dendritic targets of M2R-labeled terminals

The observed contacts between M2R-labeled terminals and dendrites expressing DAT suggest that M2R agonists may influence the presynaptic release of diverse neurotransmitters (see prior section) onto dopaminergic neurons in the VTA. The M2R-labeled terminals making asymmetric synapses onto VTA dopamine neurons are presumably originating from (1) cholinergic mesopontine neurons (Henderson and Sheriff, 1991; Oakman et al., 1995; Garzón et al., 1999), whose stimulation produces an increase in dopamine release in targets of VTA neurons (Niijima and Yoshida, 1988), or (2) cortical neurons containing excitatory amino acids (Christie et al., 1985; Sesack et al., 1989; Sesack and Pickel, 1992) impinging most specifically on mesocortical VTA dopaminergic neurons (Sesack et al., 1998; Carr and Sesack, 2000).

The M2R were also detected in terminals contacting dendrites that contained M2R, but not DAT immunoreactivity. These terminals were morphologically heterogeneous and may contain acetylcholine or other neurotransmitters including excitatory and inhibitory amino

acids (see above discussion). Both glutamate and acetylcholine have been shown to depolarize VTA neurons (for review see Adell and Artigas, 2004). Taken together, these data indicate that M2R activation in VTA cells can modulate pre- as well as postsynaptic responses of presumed GABA-containing neurons to inhibitory and excitatory inputs. These GABA-containing neurons may locally inhibit dopaminergic neurons and/or project to corticolimbic areas. In the cortex and hippocampus, acetylcholine has been shown to inhibit GABA release from axon terminals through M2R activation (Ferraro et al., 1997; Fukudome et al., 2004). Comparable GABA release inhibition through M2R has been reported in the nucleus accumbens in vitro (Ferraro et al., 1996).

Conclusion

Our results establish that in the rat VTA, M2 receptors have a prominent size-dependent plasmalemmal distribution in non-dopaminergic neurons, but also are expressed within the cytoplasm of a few dopaminergic somata and dendrites. In addition, M2R are located presynaptically in morphologically heterogeneous axon terminals providing input to the dopaminergic and non-dopaminergic neurons (Fig. 10). Collectively, these observations identify crucial pre- and postsynaptic sites in the VTA where activation of M2R can affect cognitive and goal-based dopamine-mediated behaviors (Hulme et al., 1990).

Acknowledgments

References

Adell A, Artigas F. The somatodendritic release of dopamine in the ventral tegmental area and its regulation by afferent transmitter systems. Neurosci Biobehav Rev. 2004; 28:415–431. [PubMed: 15289006]

Alcantara AA, Mrzljak L, Jakab RL, Levey AI, Hersch SM, Goldman-Rakic PS. Muscarinic m1 and m2 receptor proteins in local circuit and projection neurons of the primate striatum: anatomical evidence for cholinergic modulation of glutamatergic prefronto-striatal pathways. J Comp Neurol. 2001; 434:445–460. [PubMed: 11343292]

Asztely F, Erdemli G, Kullmann DM. Extrasynaptic glutamate spillover in the hippocampus: dependence on temperature and the role of active glutamate uptake. Neuron. 1997; 18:281–293. [PubMed: 9052798]

Baghdoyan HA, Lydic R, Fleegal MA. M2 muscarinic autoreceptors modulate acetylcholine release in the medial pontine reticular formation. J Pharmacol Exp Ther. 1998; 286:1446–1452. [PubMed: 9732410]

Baude Z, Nusser Z, Roberts JD, Mulvihill E, McIlhinney RA, Somogyi P. The metabotropic glutamate receptor (mGluR1 alpha) is concentrated at perisynaptic membrane of neuronal subpopulations as detected by immunogold reaction. Neuron. 1993; 11:771–787. [PubMed: 8104433]

Bernard V, Laribi O, Levey AI, Bloch B. Subcellular redistribution of m2 muscarinic acetylcholine receptors in striatal interneurons in vivo after acute cholinergic stimulation. J Neurosci. 1998; 18:10207–10218. [PubMed: 9822774]

Bonner TI, Buckley NJ, Young AC, Brann MR. Identification of a family of muscarinic acetylcholine receptor genes. Science. 1987; 237:527–532. [PubMed: 3037705]

Bonner TI, Young AC, Brann MR, Buckley NJ. Cloning and expression of the human and rat m5 muscarinic acetylcholine receptor genes. Neuron. 1988; 1:403–410. [PubMed: 3272174]

Bourne HR. Do GTPases direct membrane traffic in secretion? Cell. 1988; 53:669–671. [PubMed: 2836065]

Bradbury NA, Bridges RJ. Role of membrane trafficking in plasma membrane solute transport. Am J Physiol. 1994; 267:C1–C24. [PubMed: 7519393]

Broadwell RD, Cataldo AM. The neuronal endoplasmic reticulum: its cytochemistry and contribution to the endomembrane system. I. Cell bodies and dendrites. J Histochem Cytochem. 1983; 31:1077–1088. [PubMed: 6309951]

Buckley NJ, Bonner TI, Brann MR. Localization of a family of muscarinic receptor mRNAs in rat brain. J Neurosci. 1988; 8:4646–4652. [PubMed: 3199198]

Cahill CM, Morinville A, Lee MC, Vincent JP, Collier B, Beaudet A. Prolonged morphine treatment targets δ opioid receptors to neuronal plasma membranes and enhances δ-mediated antinociception. J Neurosci. 2001; 21:7598–7607. [PubMed: 11567050]

Carr DB, Sesack SR. GABA-containing neurons in the rat ventral tegmental area project to the prefrontal cortex. Synapse. 2000; 38:114–123. [PubMed: 11018785]

Chan J, Aoki C, Pickel VM. Optimization of differential immunogold-silver and peroxidase labeling with maintenance of ultrastructure in brain sections before plastic embedding. J Neurosci Methods. 1990; 33:113–127. [PubMed: 1977960]

Charara A, Smith Y, Parent A. Glutamatergic inputs from the pedunculopontine nucleus to midbrain dopaminergic neurons in primates: Phaseolus vulgaris-leucoagglutinin anterograde labeling combined with postembedding glutamate and GABA immunohistochemistry. J Comp Neurol. 1996; 364:254–266. [PubMed: 8788248]

Ciliax BJ, Drash GW, Staley JK, Haber S, Mobley CJ, Miller GW, Mufson EJ, Mash DC, Levey AI. Immunocytochemical localization of the dopamine transporter in human brain. J Comp Neurol. 1999; 409:38–56. [PubMed: 10363710]

Ciliax BJ, Heilman C, Demchyshyn LL, Pristupa ZB, Ince E, Hersch SM, Niznik HB, Levey AI. The dopamine transporter: immunochemical characterization and localization in brain. J Neurosci. 1995; 15:1714–1723. [PubMed: 7534339]

Christie MJ, Bridge S, James LB, Beart PM. Excitotoxin lesions suggest an aspartatergic projection from rat medial prefrontal cortex to ventral tegmental area. Brain Res. 1985; 333:169–172. [PubMed: 2859910]

Clader JW, Wang Y. Muscarinic receptor agonists and antagonists in the treatment of Alzheimer's disease. Curr Pharm Des. 2005; 11:3353–3361. [PubMed: 16250841]

Comings DE, Wu S, Rostamkhani M, McGue M, Iacono WG, Cheng LS, MacMurray JP. Role of the cholinergic muscarinic 2 receptor (CHRM2) gene in cognition. Mol Psychiatry. 2003; 8:10–11. [PubMed: 12556901]

Decossas M, Bloch B, Bernard V. Trafficking of the muscarinic m2 autoreceptor in cholinergic basalocortical neurons in vivo: differential regulation of plasma membrane receptor availability and intraneuronal localization in acetylcholinesterase-deficient and -inhibited mice. J Comp Neurol. 2003; 462:302–314. [PubMed: 12794734]

Dolphin AC. Voltage-dependent calcium channels and their modulation by neurotransmitters and G proteins. Exp Physiol. 1995; 80:1–36. [PubMed: 7734129]

Dolphin AC. Mechanisms of modulation of voltage-dependent calcium channels by G proteins. J Physiol. 1998; 506:3–11. [PubMed: 9481669]

Douglas CL, Baghdoyan HA, Lydic R. M2 muscarinic autoreceptors modulate acetylcholine release in prefrontal cortex of C57BL/6J mouse. J Pharmacol Exp Ther. 2001; 299:960–966. [PubMed: 11714883]

Enrico P, Bouma M, De Vries JB, Westerink BHC. The role of afferents to the ventral tegmental area in the handling stress-induced increase in the release of dopamine in the medial prefrontal cortex: a dual-probe microdialysis in the rat brain. Brain Res. 1998; 779:205–213. [PubMed: 9473673]

Erisir A, Levey AI, Aoki C. Muscarinic receptor M(2) in cat visual cortex: laminar distribution, relationship to gamma-aminobutyric acidergic neurons, and effect of cingulate lesions. J Comp Neurol. 2001; 441:168–185. [PubMed: 11745643]

Ferraro L, Beani L, Bianchi C, Tanganelli S. Inhibitory cholinergic control of endogenous GABA release from electrically stimulated cortical slices and K(+)-depolarized synaptosomes. Neurochem Int. 1997; 31:795–800. [PubMed: 9413841]

Ferraro L, O'Connor WT, Li XM, Rimondini R, Beani L, Ungerstedt U, Fuxe K, Tanganelli S. Evidence for a differential cholecystokinin-B and -A receptor regulation of GABA release in the rat nucleus accumbens mediated via dopaminergic and cholinergic mechanisms. Neuroscience. 1996; 73:941–50. [PubMed: 8809813]

Forster GL, Blaha CD. Laterodorsal tegmental stimulation elicits dopamine efflux in the rat nucleus accumbens by activation of acetylcholine and glutamate receptors in the ventral tegmental area. Eur J Neurosci. 2000; 12:3596–3604. [PubMed: 11029630]

Forster GL, Blaha CD. Pedunculopontine tegmental stimulation evokes striatal dopamine efflux by activation of acetylcholine and glutamate receptors in the midbrain and pons of the rat. Eur J Neurosci. 2003; 17:751–762. [PubMed: 12603265]

Fukudome Y, Ohno-Shosaku T, Matsui M, Omori Y, Fukaya M, Tsubokawa H, Taketo MM, Watanabe M, Manabe T, Kano M. Two distinct classes of muscarinic action on hippocampal inhibitory synapses: M2-mediated direct suppression and M1/M3-mediated indirect suppression through endocannabinoid signalling. Eur J Neurosci. 2004; 19:2682–2692. [PubMed: 15147302]

Garzón M, Vaughan RA, Uhl GR, Kuhar MJ, Pickel VM. Cholinergic axon terminals in the ventral tegmental area target a subpopulation of neurons expressing low levels of the dopamine transporter. J Comp Neurol. 1999; 410:197–210. [PubMed: 10414527]

Gomeza J, Shannon H, Kostenis E, Felder C, Zhang L, Brodkin J, Grinberg A, Sheng H, Wess J. Pronounced pharmacologic deficits in M2 muscarinic acetylcholine receptor knockout mice. Proc Natl Acad Sci USA. 1999; 96:1692–1697. [PubMed: 9990086]

Gomeza J, Zhang L, Kostenis E, Felder CC, Bymaster FP, Brodkin J, Shannon H, Xia B, Duttaroy A, Deng CX, Wess J. Generation and pharmacological analysis of M2 and M4 muscarinic receptor knockout mice. Life Sci. 2001; 68:2457–2466. [PubMed: 11392613]

Gray EG. Axosomatic and axo-dendritic synapses of the cerebral cortex: an electron microscopic study. J Anat. 1959; 93:420–433. [PubMed: 13829103]

Greba Q, Munro LJ, Kokkinidis L. The involvement of ventral tegmental area cholinergic muscarinic receptors in classically conditioned fear expression as measured with fear-potentiated startle. Brain Res. 2000; 870:135–141. [PubMed: 10869510]

Grillner P, Mercuri NB. Intrinsic membrane properties and synaptic inputs regulating the firing activity of the dopamine neurons. Behav Brain Res. 2002; 130:149–169. [PubMed: 11864731]

Gronier B, Perry KW, Rasmussen K. Activation of the mesocorticolimbic dopaminergic system by stimulation of muscarinic cholinergic receptors in the ventral tegmental area. Psychopharmacology. 2000; 147:347–355. [PubMed: 10672627]

Gronier B, Rasmussen K. Activation of midbrain presumed dopaminergic neurones by muscarinic cholinergic receptors: an *in vivo* electrophysiological study in the rat. British J Pharmacol. 1998; 124:455–464.

Henderson Z, Sherriff FE. Distribution of choline acetyltransferase immunoreactive axons and terminals in the rat and ferret brainstem. J Comp Neurol. 1991; 314:147–163. [PubMed: 1797870]

Hersch SM, Gutekunst CA, Rees HD, Heilman CJ, Levey AI. Distribution of m1-m4 muscarinic receptor proteins in the rat striatum: light and electron microscopic immunocytochemistry using subtype-specific antibodies. J Neurosci. 1994; 14:3351–3363. [PubMed: 8182478]

Hersch SM, Yi H, Heilman CJ, Edwards RH, Levey AI. Subcellular localization and molecular topology of the dopamine transporter in the striatum and substantia nigra. J Comp Neurol. 1997; 388:211–227. [PubMed: 9368838]

Hsu SM, Raine L, Fanger H. The use of avidin-biotin-peroxidase complex (ABC) in immunoperoxidase technique: a comparison between ABC and unlabeled antibody (peroxidase) procedures. J Histochem Cytochem. 1981; 29:577–599. [PubMed: 6166661]

Hulme EC, Birdsall NJ, Buckley NJ. Muscarinic receptor subtypes. Annu Rev Pharmacol Toxicol. 1990; 30:633–673. [PubMed: 2188581]

Ikemoto S, Wise RA. Rewarding effects of the cholinergic agents carbachol and neostigmine in the posterior ventral tegmental area. J Neurosci. 2002; 22:9895–9904. [PubMed: 12427846]

Ikemoto S, Witkin BM, Morales M. Rewarding injections of the cholinergic agonist carbachol into the ventral tegmental area induce locomotion and c-Fos expression in the retrosplenial area and supramammillary nucleus. Brain Res. 2003; 969:78–87. [PubMed: 12676367]

Kayadjian N, Gioanni H, Menetrey A, Besson MJ. Muscarinic receptor stimulation increases the spontaneous [3H]GABA release in the rat substantia nigra through muscarinic receptors localized on striatonigral terminals. Neuroscience. 1994; 63:989–1002. [PubMed: 7700520]

Kilbinger H. Presynaptic muscarinic receptors modulating acetylcholine release. Trends Pharmacol Sci. 1984; 5:103–105.

Kitaichi K, Hori T, Srivastava LK, Quirion R. Antisense oligodeoxynucleotides against the muscarinic m2, but not m4, receptor supports its role as autoreceptors in the rat hippocampus. Mol Brain Res. 1999; 67:98–106. [PubMed: 10101237]

van Koppen CJ. Multiple pathways for the dynamin-regulated internalization of muscarinic acetylcholine receptors. Biochem Soc Trans. 2001; 29:505–508. [PubMed: 11498018]

Krudewig R, Langer B, Vogler O, Markschies N, Erl M, Jakobs KH, van Koppen CJ. Distinct internalization of M2 muscarinic acetylcholine receptors confers selective and long-lasting desensitization of signaling to phospholipase C. J Neurochem. 2000; 74:1721–1730. [PubMed: 10737631]

Kubo T, Fukuda K, Mikami A, Maeda A, Takahashi H, Mishina M, Haga T, Haga K, Ichiyama A, Kangawa K, Kojima M, Matsuo H, Hirose T, Numa S. Cloning, sequencing and expression of complementary DNA encoding the muscarinic acetylcholine receptor. Nature. 1986; 323:411–416. [PubMed: 3762692]

Lacey MG, Calabresi P, North RA. Muscarine depolarizes rat substantia nigra zona compacta and ventral tegmental neurons in vitro through M_1-like receptors. J Pharmacol Exp Ther. 1990; 253:395–400. [PubMed: 2329522]

Langer SZ. 25 years since the discovery of presynaptic receptors: present knowledge and future perspectives. Trends Pharmacol Sci. 1997; 18:95–99. [PubMed: 9133779]

Leranth, C.; Pickel, VM. Electron microscopic pre-embedding double immnunostaining methods. In: Heimer, L.; Zaborsky, L., editors. Tract tracing methods 2, recent progress. New York: Plenum; 1989. p. 129-172.

Levey AI, Kitt CA, Simonds WF, Price DL, Brann MR. Identification and localization of muscarinic acetylcholine receptor proteins in brain with subtype-specific antibodies. J Neurosci. 1991; 11:3218–3226. [PubMed: 1941081]

Li DP, Chen SR, Pan YZ, Levey AI, Pan HL. Role of presynaptic muscarinic and GABA$_B$ receptors in glutamate release and cholinergic analgesia in rats. J Physiol. 2002; 543:807–818. [PubMed: 12231640]

Luján R, Nusser Z, Roberts JD, Shigemoto R, Somogyi P. Perisynaptic location of metabotropic glutamate receptors mGluR1 and mGluR5 on dendrites and dendritic spines in the rat hippocampus. Eur J Neurosci. 1996; 8:1488–1500. [PubMed: 8758956]

Miller AD, Forster GL, Yeomans JS, Blaha CD. Midbrain muscarinic receptors modulate morphine-induced accumbal and striatal dopamine efflux in the rat. Neuroscience. 2005; 136:531–8. [PubMed: 16216430]

Miller GW, Staley JK, Heilman CJ, Perez JT, Mash DC, Rye DB, Levey AI. Immunochemical analysis of dopamine transporter protein in Parkinson's disease. Ann Neurol. 1997; 41:530–539. [PubMed: 9124811]

Mizoguchi A, Kim S, Ueda T, Kikuchi A, Yorifuji H, Hirokawa N, Takai Y. Localization and subcellular distribution of smg p25A, a ras p21-like GTP-binding protein, in rat brain. J Biol Chem. 1990; 265:11872–11879. [PubMed: 2114404]

Mrzljak L, Levey AI, Belcher S, Goldman-Rakic PS. Localization of the m2 muscarinic acetylcholine receptor protein and mRNA in cortical neurons of the normal and cholinergically deafferented rhesus monkey. J Comp Neurol. 1998; 390:112–132. [PubMed: 9456180]

Mrzljak L, Levey AI, Goldman-Rakic PS. Association of m1 and m2 muscarinic receptor proteins with asymmetric synapses in the primate cerebral cortex: morphological evidence for cholinergic modulation of excitatory neurotransmission. Proc Natl Acad Sci USA. 1993; 90:5194–5198. [PubMed: 8389473]

Mukherjee S, Ghosh RN, Maxfield FR. Endocytosis. Physiol Rev. 1997; 77:759–803. [PubMed: 9234965]

Nijima K, Yoshida M. Activation of mesencephalic dopamine neurons by chemical stimulation of the nucleus tegmenti pedunculopontinus pars compacta. Brain Res. 1988; 451:163–71. [PubMed: 3251582]

Nusser Z, Roberts JD, Baude A, Richards JG, Somogyi P. Relative densities of synaptic and extrasynaptic GABAA receptors on cerebellar granule cells as determined by a quantitative immunogold method. J Neurosci. 1995; 15:2948–2960. [PubMed: 7722639]

Oakman SA, Faris PL, Kerr PE, Cozzari C, Hartman BK. Distribution of pontomesencephalic cholinergic neurons projecting to substantia nigra differs significantly from those projecting to ventral tegmental area. J Neurosci. 1995; 15:5859–5869. [PubMed: 7666171]

Paquet M, Tremblay M, Soghomonian JJ, Smith Y. AMPA and NMDA glutamate receptor subunits in midbrain dopaminergic neurons in the squirrel monkey: an immunohistochemical and in situ hybridization study. J Neurosci. 1997; 17:1377–1396. [PubMed: 9006980]

Parton RG, Simons K, Dotti CG. Axonal and dendritic endocytic pathways in cultured neurons. J Cell Biol. 1992; 119:123–137. [PubMed: 1527164]

Paxinos, G.; Watson, C. The Rat Brain in Stereotaxic Coordinates. San Diego: Academic Press Inc; 1986.

Peralta EG, Winslow JW, Peterson GL, Smith DH, Ashkenazi A, Ramachandran J, Schimerlik MI, Capon DJ. Primary structure and biochemical properties of an M2 muscarinic receptor. Science. 1987; 236:600–605. [PubMed: 3107123]

Peters, A.; Palay, SL.; Webster, HD. The fine structure of the nervous system: neurons and their supporting cells. Oxford: Oxford University Press; 1991.

Phillipson OT. Afferent projections to the ventral tegmental area of Tsai and interfascicular nucleus: a horseradish peroxidase study in the rat. J Comp Neurol. 1979; 187:117–143. [PubMed: 489776]

Pickel VM, Chan J, Sesack SR. Cellular substrates for interactions between dynorphin terminals and dopamine dendrites in rat ventral tegmental area and substantia nigra. Brain Res. 1993; 602:275–289. [PubMed: 8095430]

Prensa L, Parent A. The nigrostriatal pathway in the rat: A single-axon study of the relationship between dorsal and ventral tier nigral neurons and the striosome/matrix striatal compartments. J Neurosci. 2001; 21:7247–60. [PubMed: 11549735]

Pristupa ZB, Wilson JM, Hoffman BJ, Kish SJ, Niznik HB. Pharmacological heterogeneity of the cloned and native human dopamine transporter: disassociation of [^{3}H]WIN 35,428 and [^{3}H]GBR 12,935 binding. Mol Pharmacol. 1994; 45:125–135. [PubMed: 8302271]

Raiteri M, Marchi M, Paudice P. Presynaptic muscarinic receptors in the central nervous system. Ann N Y Acad Sci. 1990; 604:113–129. [PubMed: 1977344]

Reynolds ES. The use of lead citrate at high pH as an electron-opaque stain in electron microscopy. J Cell Biol. 1963; 17:208. [PubMed: 13986422]

Rouse ST, Edmunds SM, Yi H, Gilmor ML, Levey AI. Localization of M(2) muscarinic acetylcholine receptor protein in cholinergic and non-cholinergic terminals in rat hippocampus. Neurosci Lett. 2000; 284:182–186. [PubMed: 10773429]

Rouse ST, Gilmor ML, Levey AI. Differential presynaptic and postsynaptic expression of m1-m4 muscarinic acetylcholine receptors at the perforant pathway/granule cell synapse. Neuroscience. 1998; 86:221–232. [PubMed: 9692756]

Rouse ST, Thomas TM, Levey AI. Muscarinic acetylcholine receptor subtype, m2: diverse functional implications of differential synaptic localization. Life Sci. 1997; 60:1031–1038. [PubMed: 9121344]

Sesack SR, Deutch AY, Roth RH, Bunney BS. Topographical organization of the efferent projections of the medial prefrontal cortex in the rat: An anterograde tract-tracing study with *Phaseolus vulgaris*-leucoagglutinin. J Comp Neurol. 1989; 290:213–242. [PubMed: 2592611]

Sesack SR, Hawrylak VA, Matus C, Guido MA, Levey AI. Dopamine axon varicosities in the prelimbic division of the rat prefrontal cortex exhibit sparse immunoreactivity for the dopamine transporter. J Neurosci. 1998; 18:2697–2708. [PubMed: 9502827]

Sesack SR, Pickel VM. Prefrontal cortical efferents in the rat synapse on unlabeled neuronal targets of catecholamine terminals in the nucleus accumbens septi and on dopamine neurons in the ventral tegmental area. J Comp Neurol. 1992; 320:145–160. [PubMed: 1377716]

Sesack SR, Pickel VM. Ultrastructural relationships between terminals immunoreactive for enkephalin, GABA, or both transmitters in the rat ventral tegmental area. Brain Res. 1995; 672:261–275. [PubMed: 7538419]

Shapiro MS, Gomeza J, Hamilton SE, Hille B, Loose MD, Nathanson NM, Roche JP, Wess J. Identification of subtypes of muscarinic receptors that regulate Ca2+ and K+ channel activity in sympathetic neurons. Life Sci. 2001; 68:2481–2487. [PubMed: 11392616]

Shapiro MS, Loose MD, Hamilton SE, Nathanson NM, Gomeza J, Wess J, Hille B. Assignment of muscarinic receptor subtypes mediating G-protein modulation of Ca(2+) channels by using knockout mice. Proc Natl Acad Sci USA. 1999; 96:10899–10904. [PubMed: 10485923]

Smiley JF, Levey AI, Mesulam MM. m2 muscarinic receptor immunolocalization in cholinergic cells of the monkey basal forebrain and striatum. Neuroscience. 1999; 90:803–814. [PubMed: 10218781]

Smith Y, Charara A, Parent A. Synaptic innervation of midbrain dopaminergic neurons by glutamate-enriched terminals in the squirrel monkey. J Comp Neurol. 1996; 364:231–253. [PubMed: 8788247]

Smythe E, Warren G. The mechanism of receptor-mediated endocytosis. Eur J Biochem. 1991; 202:689–699. [PubMed: 1662613]

Starke K, Gothert M, Kilbinger H. Modulation of neurotransmitter release by presynaptic autoreceptors. Physiol Rev. 1989; 69:864–989. [PubMed: 2568648]

Steffensen SC, Svingos AL, Pickel VM, Henriksen SJ. Electrophysiological characterization of GABAergic neurons in the ventral tegmental area. J Neurosci. 1998; 18:8003–8015. [PubMed: 9742167]

Stowell JN, Craig AM. Axon/dendrite targeting of metabotropic glutamate receptors by their cytoplasmic carboxy-terminal domains. Neuron. 1999; 22:525–536. [PubMed: 10197532]

Sudhof TC. The synaptic vesicle cycle. Annu Rev Neurosci. 2004; 27:509–547. [PubMed: 15217342]

Svingos AL, Clarke CL, Pickel VM. Localization of the delta-opioid receptor and dopamine transporter in the nucleus accumbens shell: implications for opiate and psychostimulant cross-sensitization. Synapse. 1999; 34:1–10. [PubMed: 10459166]

Svingos AL, Chavkin C, Colago EE, Pickel VM. Major coexpression of kappa-opioid receptors and the dopamine transporter in nucleus accumbens axonal profiles. Synapse. 2001; 42:185–192. [PubMed: 11746715]

Ushijima I, Mizuki Y, Kobayashi T, Aoki T, Suetsugi M, Usami K, Watanabe Y. Effects of pertussis toxin on behavioral responses during different withdrawal periods from chronic cocaine treatment. Prog Neuropsychopharmacol Biol Psychiatry. 2000; 24:1369–77. [PubMed: 11125860]

Van Bockstaele EJ, Pickel VM. GABA-containing neurons in the ventral tegmental area project to the nucleus accumbens in rat brain. Brain Res. 1995; 682:215–221. [PubMed: 7552315]

Vannucchi MG, Pepeu G. Muscarinic receptor modulation of acetylcholine release from rat cerebral cortex and hippocampus. Neurosci Lett. 1995; 190:53–56. [PubMed: 7624055]

Vilaró MT, Palacios JM, Mengod G. Multiplicity of muscarinic autoreceptor subtypes? Comparison of the distribution of cholinergic cells and cells containing mRNA for five subtypes of muscarinic receptors in the rat brain. Mol Brain Res. 1994; 21:30–46. [PubMed: 8164520]

Vilaró MT, Wiederhold KH, Palacios JM, Mengod G. Muscarinic M2 receptor mRNA expression and receptor binding in cholinergic and non-cholinergic cells in the rat brain: a correlative study using in situ hybridization histochemistry and receptor autoradiography. Neuroscience. 1992; 47:367–393. [PubMed: 1641129]

Vizi ES. Role of high-affinity receptors and membrane transporters in nonsynaptic communication and drug action in the central nervous system. Pharmacol Rev. 1998; 52:63–89. [PubMed: 10699155]

Vizi ES, Kiss JP. Neurochemistry and pharmacology of the major hippocampal transmitter systems: synaptic and nonsynaptic interactions. Hippocampus. 1998; 8:566–607. [PubMed: 9882017]

Weclewicz K, Svensson L, Kristensson D. Targeting of endoplasmic reticulum-associated proteins to axons and dendrites in rotavirus-infected neurons. Brain Res Bull. 1998; 46:353–360. [PubMed: 9671265]

Weiner DM, Brann MR. Distribution of m1-m5 muscarinic receptor mRNAs in rat brain. TIPS (Suppl). 1989; 10:115.

Weiner DM, Levey AI, Brann MR. Expression of muscarinic acetylcholine and dopamine receptor mRNAs in rat basal ganglia. Proc Natl Acad Sci USA. 1990; 87:7050–7054. [PubMed: 2402490]

Wess J, Duttaroy A, Gomeza J, Zhang W, Yamada M, Felder CC, Bernardini N, Reeh PW. Muscarinic receptor subtypes mediating central and peripheral antinociception studied with muscarinic receptor knockout mice: a review. Life Sci. 2003; 72:2047–2054. [PubMed: 12628455]

Westerink BH, Enrico P, Feimann J, De Vries JB. The pharmacology of mesocortical dopamine neurons: a dual-probe microdialysis study in the ventral tegmental area and prefrontal cortex of the rat brain. J Pharmacol Exp Ther. 1998; 285:143–154. [PubMed: 9536004]

Westerink BHC, Kwint HF, De Vries JB. The pharmacology of mesolimbic dopamine neurons: a dual-probe microdialysis study in the ventral tegmental area and nucleus accumbens of the rat brain. J Neurosci. 1996; 16:2605–2611. [PubMed: 8786436]

Yamada M, Lamping KG, Duttaroy A, Zhang W, Cui Y, Bymaster FP, McKinzie DL, Felder CC, Deng CX, Faraci FM, Wess J. Cholinergic dilation of cerebral blood vessels is abolished in M(5) muscarinic acetylcholine receptor knockout mice. Proc Natl Acad Sci USA. 2001; 98:14096–14101. [PubMed: 11707605]

Yeomans JS. Role of tegmental cholinergic neurons in dopaminergic activation, antimuscarinic psychosis and schizophrenia. Neuropsychopharmacology. 1995; 12:3–16. [PubMed: 7766284]

Yeomans J, Baptista M. Both nicotinic and muscarinic receptors in ventral tegmental area contribute to brain-stimulation reward. Pharmacol Biochem Behav. 1997; 57:915–921. [PubMed: 9259024]

Youdim MB, Buccafusco JJ. CNS Targets for multi-functional drugs in the treatment of Alzheimer's and Parkinson's diseases. J Neural Transm. 2005; 112:519–537. [PubMed: 15666041]

Zhang W, Basile AS, Gomeza J, Volpicelli LA, Levey AI, Wess J. Characterization of central inhibitory muscarinic autoreceptors by the use of muscarinic acetylcholine receptor knock-out mice. J Neurosci. 2002; 22:1709–1717. [PubMed: 11880500]

Abbreviations

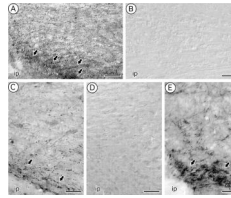|	
ABC	avidin-biotin complex
BSA	bovine serum albumin
DAT	dopamine transporter
M2R	muscarinic M2 receptor(s)
PB	phosphate buffer
PBS	phosphate-buffered saline
TS	Tris-buffered saline
VTA	ventral tegmental area

Figure 1.
Specific M2-immunoreactivity is expressed in the VTA. **A:** Distribution of m2-immunoreactivity in the neuropil of a wild-type rat VTA section at –5.60 mm AP level from Bregma, as indicated in Paxinos & Watson atlas. A dense punctate or varicose labeling (arrows) is observed throughout the VTA, mainly in the paranigral sector adjacent to interpeduncular nucleus (ip). **B:** Immunogen fusion protein adsorption shows no specific labeling in an adjacent tissue section processed under the same labeling condition, except for the use of anti-m2R antiserum preadsorbed with the antigenic fusion protein (3 μg fusion protein per 1 μg anti-m2R). **C:** Distribution of m2-immunoreactivity in the neuropil of a wild-type mouse VTA. Varicose m2 immunolabeling (arrows) was localized mainly to paranigral region of the VTA, as was the case for rats (A). **D:** Similar immunohistochemical processing in same AP level tissue section of a m2 null mice shows complete lack of fiber-like varicose processes, demonstrating absence of specific m2-immunoreactivity. **E:** m2-immunoreactivity (arrows) is conserved in an analogous AP level VTA section of a m5 null mice. ip, interpeduncular nucleus. Scale bars, 25 μm.
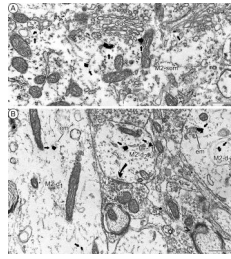
Figure 2.
Endomembrane immunogold M2 receptor distribution in somata and dendrites without DAT. **A:** M2-immunogold particles (straight arrows) are seen distributed in the cytoplasm near to the Golgi complex (Go) within a neuronal soma (M2-som). **B:** Large dendrites sectioned in a longitudinal (M2-d_1) or a transverse (M2-d_{2-3}) planes show cytoplasmic immunogold-M2 particles (straight black arrows) distributed mainly near endomembranes (em). The smaller dendrite (M2-d_2) receives an asymmetric synapse (curved black arrow) from an unlabeled terminal and also shows immunogold-M2 labeling (straight black arrows) in contact with the cytoplasmic surface of the plasma membrane. Scale bars = 0.5 μm.
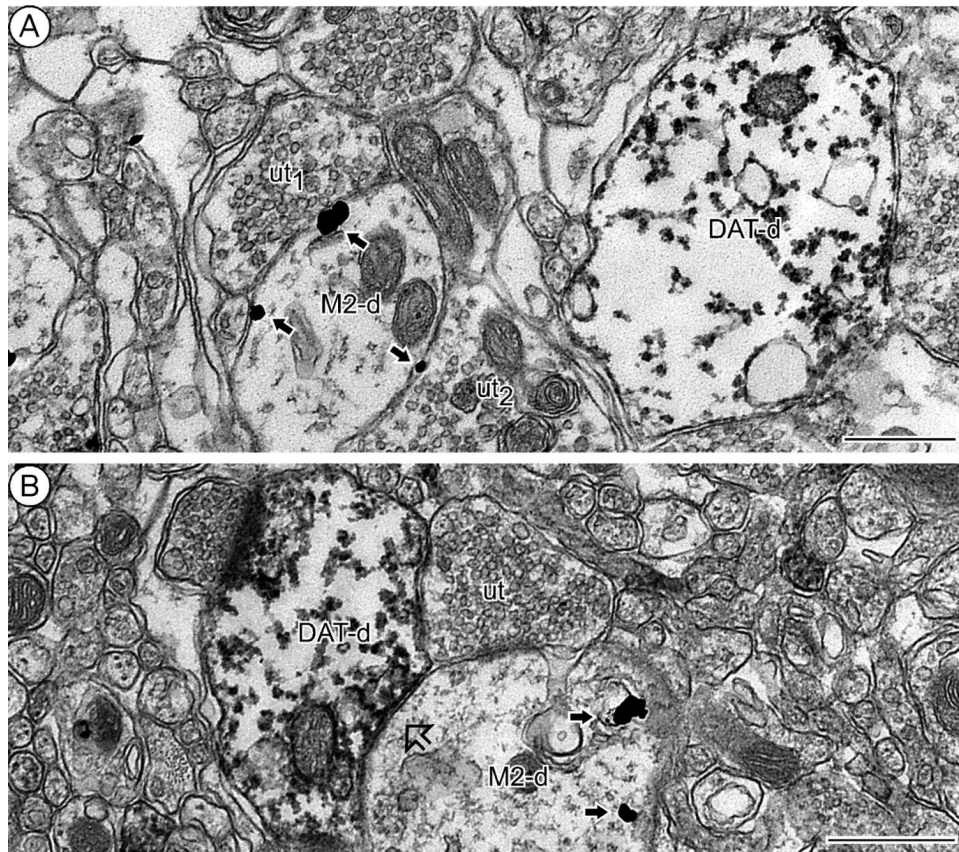
Figure 3.
Plasmalemmal M2 receptor distribution in non-dopaminergic dendrites. **A:** M2-immunogold particles (straight black arrows) are exclusively localized to the plasma membrane of a dendrite (M2-d) distinct from a nearby dendrite containing peroxidase labeling for DAT (DAT-d). The gold particles are located within and near contacts from unlabeled terminals (ut$_{1-2}$). **B:** Unlabeled terminal (ut) establishes contacts with two differentially labeled and apposing (block arrow) dendrites; one is a M2-immunoreactive dendrite (M2-d) showing M2-immunogold particles (straight black arrows) and the other is a DAT-immunolabeled dendrite (DAT-d) containing DAT-immunoperoxidase reaction product. Scale bars = 0.5 μm.
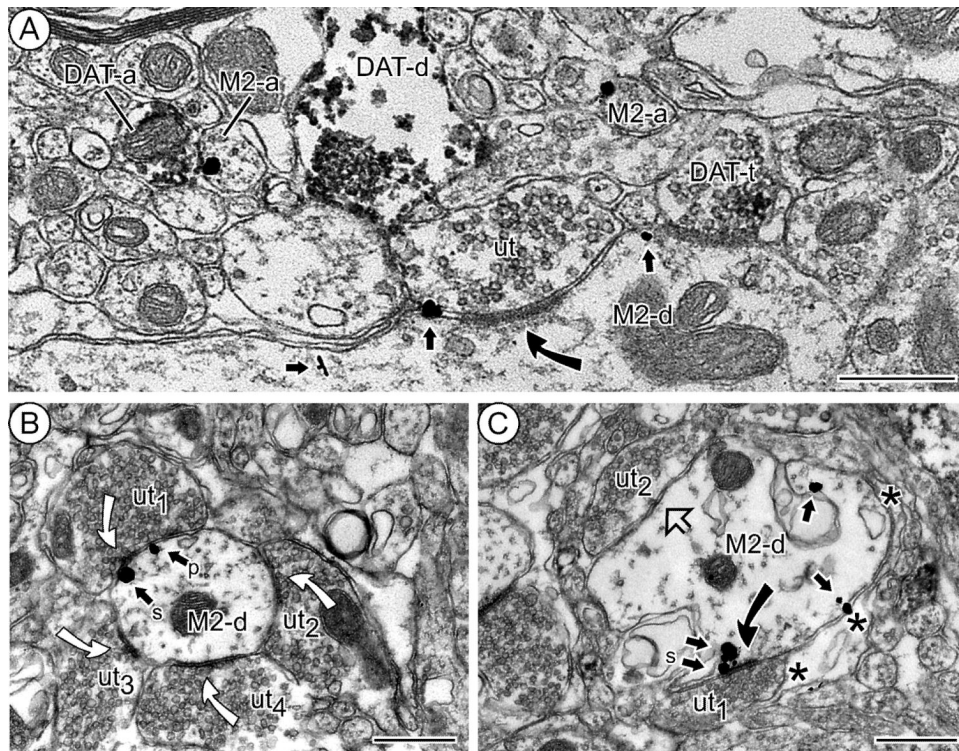
Figure 4.

Perisynaptic and synaptic locations of M2 receptor in VTA dendrites. **A:** M2-immunogold particles (straight arrows) are distributed on perisynaptic portions of a dendritic (M2-d) plasma membrane receiving an asymmetric input (curved black arrow) from an unlabeled terminal (ut). The dendrite also is contacted by a DAT-immunoperoxidase labeled axon terminal (DAT-t). In the surrounding neuropil, M2-immunogold (straight arrows) is seen on the plasma membranes of small axons (M2-a), one of which is apposed to another small axon containing the immunoperoxidase reaction product for DAT (DAT-a). **B:** An unlabeled terminal (ut$_1$) forms a symmetric synapse onto a small M2-immunoreactive dendrite (M2-d) in which one M2-immunogold particle is located within the synaptic specialization (black small arrow, s) and another in a perisynaptic site (black small arrow, p) around the synapse. The M2-d also receives multiple convergent symmetric synapses (curved white arrows) from other surrounding unlabeled axon terminals (ut$_{2-4}$). **C:** Unlabeled axon terminal (ut$_1$) makes an asymmetric synapse (curved black arrow) with a M2-immunolabeled dendrite (M2-d) showing synaptic (s) and non-synaptic M2-immunogold particles (black small arrows). The plasmalemmal surface of M2-d also is in contact with another unlabeled axon terminal (ut$_2$) and has extensive glial coverage (asterisks). Scale bars = 0.5 μm.
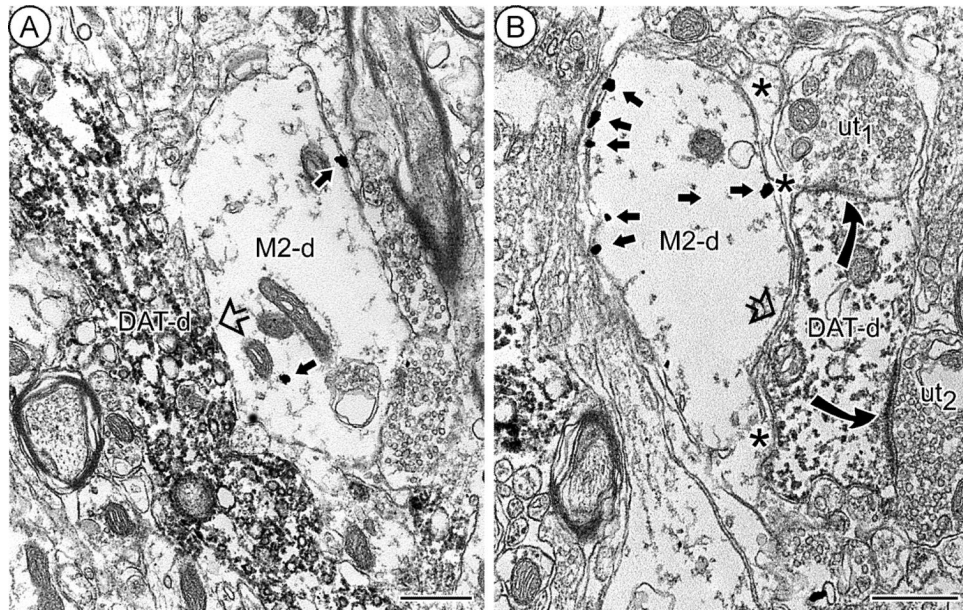
Figure 5.
M2 labeling in dendrites apposing DAT-immunoreactive dendrites. **A:** A dendrite (M2-d) showing light M2-immunogold labeling (straight arrows) makes a large appositional contact (block arrow) with a longitudinally-sectioned dendrite (DAT-d) showing intense DAT-immunoperoxidase reaction. **B:** M2-immunogold particles (straight arrows) are distributed along non-synaptic portions of a dendritic (M2-d) plasma membrane distant from a segment of the membrane adjacent to a DAT immunoperoxidase-labeled dendrite (DAT-d). The DAT-d receives input (curved black arrows) from unlabeled terminals (ut$_{1,2}$). A large astrocytic process (asterisks) precludes actual contact between the two immunoreactive dendrites, except on a small segment lacking glial intervention (block arrow). Scale bars = 0.5 μm.
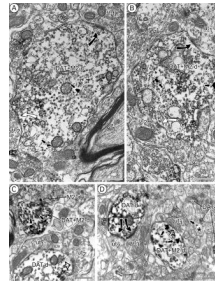
Figure 6.
Colocalization of M2 receptor and DAT in VTA dendrites. **A:** Immunoperoxidase reaction product for DAT is seen in a large dendrite (DAT+M2-d) showing sparse cytoplasmic M2-immunogold labeling. The dendrite receives both asymmetric (curved black arrow) and symmetric (curved white arrow) synapses from unlabeled terminals ($ut_{1,2}$). **B:** Unlabeled terminals ($ut_{1,2}$) establish symmetric (curved white arrow) or asymmetric (curved black arrow) synapses onto a dendrite (DAT+M2-d) containing light DAT-immunoperoxidase and M2-immunogold particles (straight arrows). **C:** A dually labeled small dendrite (DAT+M2-d) contains cytoplasmic M2-immunogold particles (straight arrows) and also intense immunoperoxidase reaction product for DAT. Another DAT-immunolabeled dendrite (DAT-d) contacting unlabeled axon terminals ($ut_{1,2}$) is seen in close proximity. M2-a, M2-immunoreactive small unmyelinated axon. **D:** An unlabeled axon terminal (ut_1) is apposed (open block arrow) to a dendrite (DAT+M2-d) showing immunoperoxidase reaction product for DAT as well as cytoplasmic M2-immunogold labeling (small black arrows). A nearby DAT-immunoreactive dendrite (DAT-d) receives convergent asymmetric inputs (curved black arrows) from unlabeled terminals ($ut_{2,3}$). In the surrounding neuropil, there are additional DAT-immunoperoxidase labeled dendrites (DAT-ds), one of which apposes a small M2-immunogold labeled (straight arrow) profile presumed to be a dendrite (asterisk). Scale bars = 0.5 μm.
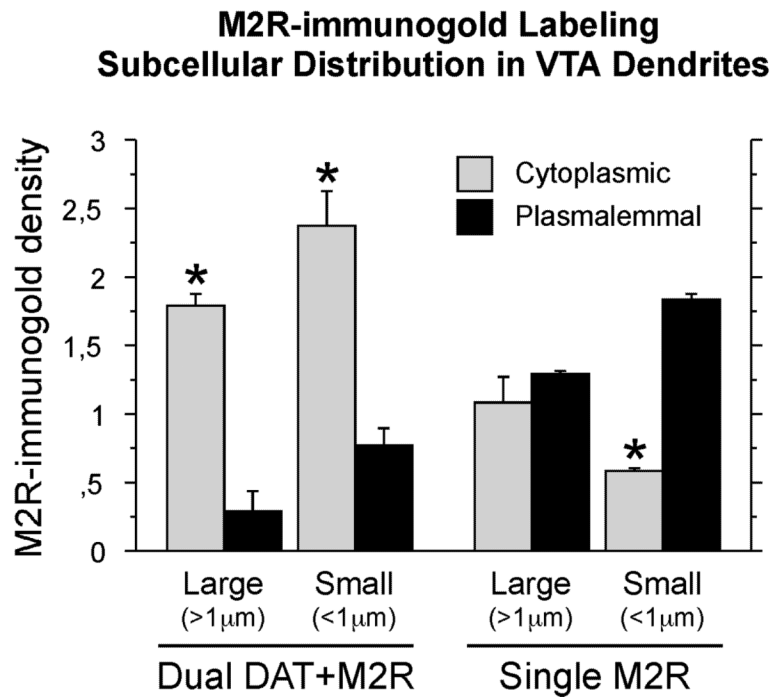
M2R-immunogold Labeling
Subcellular Distribution in VTA Dendrites

Figure 7.
Bar graph summarizing the mean±s.e. immunogold densities (number of gold particles per profile) in M2R-single and DAT+M2R-dual large (>1μm) or small (<1μm) dendrites within the VTA. Mean densities were calculated based on the numbers obtained from 746 VTA dendrites (307 large and 439 small) taken from ultrathin sections from 15 Vibratome sections in 4 rats (3084 total profiles) processed for dual labeling. *p<0.05, Fisher test for cytoplasmic versus plasmalemmal subcellular localization.
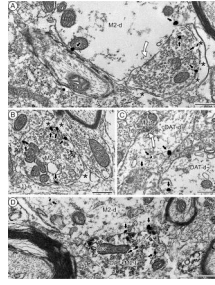
Figure 8.
M2 receptor immunogold distribution in axon terminals. **A:** Axon terminal showing immunogold particles (straight arrows) for M2 (M2-t) is encapsulated by a glial process (asterisks) and makes a symmetric synapse (curved white arrow) with a dendrite (M2-d) exhibiting plasmmalemal M2-immunogold particles (straight arrows). **B:** Axon terminal (M2-t) showing numerous plasma membrane M2-immunogold particles (straight arrows) has an extensive glial coverage (asterisks), but also contacts (block arrow) an unlabeled axon terminal (ut). dcv, dense-core vesicle. **C:** A small axon terminal showing diffuse M2-immunoperoxidase (M2-t) makes a symmetric synapse (curved white arrow) with a longitudinally-sectioned dendrite (DAT-d_1) containing DAT-immunogold particles (straight arrows). DAT-immunogold labeling (straight arrows) is also present in a nearby dendrite (DAT-d_2). **D:** A large dendrite (M2-d) showing M2-immunogold particles (straight arrows), some of which are distributed along portions of the plasma membrane is contacted by a dually-labeled axon terminal (DAT+M2-t). This terminal contains DAT immunoperoxidase and M2-immunogold particles (straight arrows) as well as small clear and large dense core vesicles (dcv). Scale bars = 0.5 μm.
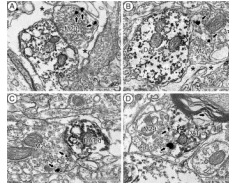
Figure 9.
M2 receptor labeling in axonal profiles contacting dopaminergic dendrites of different size.
A: DAT-peroxidase reaction product is seen in a dendrite (DAT-d) receiving input from an axon terminal (M2-t) containing M2-immunogold particles (straight arrows). Asterisks, astrocytic processes. **B:** An axon terminal (M2-t) showing cytoplasmic M2-immunogold particles (straight arrows) makes a contact (open block arrow) with a dendrite (DAT-d) containing diffuse DAT-immunoperxidase reaction product. Astrocytic leaflets partially wrap both M2-t and DAT-d. **C** and **D:** Axon terminals (M2-t) showing M2-immunogold particles (straight black arrows) contact (block arrows) DAT-immunoperoxidase labeled dendrites (DAT-d). The gold particles are located either on the plasma membrane or within the cytoplasm near synaptic vesicles. Scale bars = 0.5 μm.
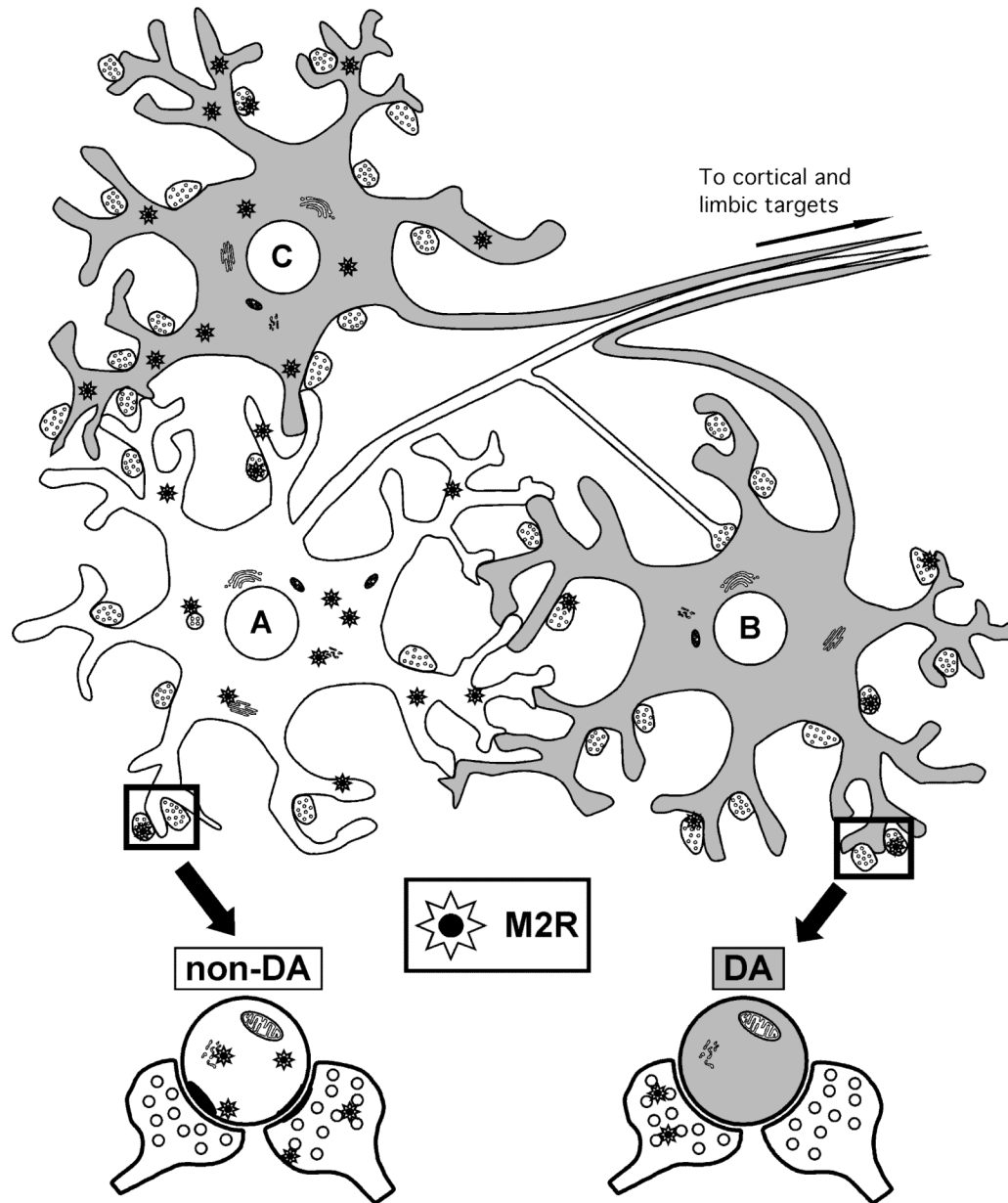
Figure 10.
Schematic diagram showing the distributions of M2 muscarinic receptors (stars) in neuronal
profiles (somata, dendrites and terminals), which express (gray filling) or not (white filling)
dopamine transporter (DAT) in the rat VTA. The M2 receptor is located mainly in non-DAT
(presumably GABA-containing) neurons (A) receiving inputs from M2-labeled and/or
unlabeled terminals. These contacts were mainly symmetric (inhibitory-type), but almost
one-third were asymmetric (excitatory-type). The DAT-containing neurons (A) of the VTA,
whose dendrites form multiple contacts with those of non-DAT neurons (B,C), usually do
not express M2 receptor (B), but receive numerous contacts from M2-immunolabeled axon
terminals. However, a minor proportion of DAT-containing neurons also express M2
receptor (C).

Table 1

Distribution of M2 and/or DAT immunolabeled cellular profiles in the VTA

TYPE OF CELLULAR PROFILE	LABELING									
	Total M2	Single M2		Dual DAT+M2		Single DAT		Total DAT		
	Number of profiles	Number of profiles	% from total M2	Number of profiles	% from total DAT	Number of profiles	% from total DAT	Number of profiles		
Dendrites	746	668	89.5	10.5	78	5.1	1452	94.9	1530	
Somata	31	28	90.3	9.7	3	33.3	6	66.7	9	
Axon Terminals	231	226	97.8	2.2	5	8.3	55	91.7	60	
Unmyelinated Axons	166	165	99.4	0.6	1	0.3	323	99.7	324	
Myelinated Axons	4	4	100	0	0	0	7	100	7	

Immunolabelings for M2 and/or DAT in different neuronal profiles within the rat VTA. Records for single M2-, single DAT- and dual DAT+M2-labelings are given as raw numbers and as percentage out from the total M2 and/or total DAT immunolabeled profiles in each category. Data were collected from 15 Vibratome sections in 4 rats processed for dual labeling.

Table 2

Statistical analysis of M2R subcellular distribution in VTA dendrites distinguished by DAT labeling and size

ASSOCIATION VARIABLES	DENDRITIC GROUP	X^2_1	p (Fisher)
Localization vs. Labeling	Small dendrites (<1μm)	126.675	<0.0001*
	Large dendrites (>1μm)	40.728	<0.0001*
Localization vs. Size	Single-labeled dendrites (M2R)	70.913	<0.0001*
	Dual-labeled dendrites (DAT+M2R)	0.974	0.4064
Labeling vs. Size	Cytoplasmic M2R localization	3.314	0.0829
	Plasmalemmal M2R localization	0.693	0.4304

Chi-square values and statistical signification (p, Fisher's exact value) for association among subcellular localization (cytoplasmic vs. plasmalemmal), type of labeling (single M2R vs. dual DAT+M2R) and dendritic size (small vs. large) of M2R-immunogold labeling observed in different groups of dendrites of the rat ventral tegmental area (VTA) with regard to those variables. A total number of 1800 M2R-immunogold particles were assessed within 746 randomly sampled VTA dendrites in 4 animals.